




 Cite this: *RSC Adv.*, 2020, **10**, 39160

Selection of a suitable ZIF-8/ionic liquid (IL) based composite for selective CO₂ capture: the role of anions at the interface†

 Anoop Thomas,  Rafiq Ahamed and Muthuramalingam Prakash *

The effective capture of CO₂ from the atmosphere is much needed to reduce its environmental impact. The design and development of CO₂ capturing materials is getting much attention. A zeolitic imidazolate framework (ZIF) can replace many of the conventional materials in gas separation due to its stability and high performance. Here, we analyzed the effect of encapsulation of ionic liquids (ILs) into the pores of ZIF-8 for selective CO₂ capture and separation. The [BMIM]⁺ cation with a series of anions was selected to study suitable carbon capture materials using density functional theory (DFT) approaches. Our calculations suggest that the nitrogen containing anions are not well adsorbed on the ZIF-8 surface but their gas separation performance is not affected by these interfacial interactions. This is confirmed from the CO₂/N₂ and CO₂/CH₄ selectivity of these composites, calculated using grand canonical Monte Carlo (GCMC) simulations. A suitable force field for the composites was identified by comparing the available force fields with the experiments. The IL@ZIF-8 composite shows better CO₂ selectivity compared to pristine ZIF-8. Fluorinated hydrophobic anions (such as [BF₄]⁻, [PF₆]⁻ and [Tf₂N]⁻) in the composites show better CO₂ adsorption and significant CO₂ selectivity than pristine ZIF-8, especially at low pressure. The nature of the anion plays an important role in CO₂ separation, rather than its stability at the pores of ZIF-8. Close scrutiny of the results reveal that the CO₂ selectivity of these composite materials depends on the anion of the IL and thus through the selection of a suitable anion we can significantly enhance the CO₂ selectivity for different flue gas mixtures. Our molecular level design shows that the selection of suitable anions in IL based composites is very important in identifying potential carbon capture materials for industrial applications.

 Received 16th September 2020
 Accepted 19th October 2020

DOI: 10.1039/d0ra07927h

rsc.li/rsc-advances

1. Introduction

Anthropogenic climate change is the main issue which the scientific community has to address. In these issues, carbon dioxide gas plays a major role.¹ According to the inter-governmental panel on climate change (IPCC), an international climate control forum under the United Nations, there has been a massive increase in CO₂ emission around the world. The recent emission gap report says, in 2018 alone, nearly 55.3 gigatons of CO₂ was pumped into the atmosphere which is 3 gigatons higher than the previous years. Also, to ensure the success of the Kyoto protocol, an agenda was proposed and followed worldwide to reduce CO₂. It is highly essential to

capture the CO₂ already effluted to the atmosphere as well as to reduce the emissions in the future; therefore it is in the urge to develop novel materials for CO₂ capture.² Also, CO₂ freezing have an adverse effect in the cryogenic natural gas processing and the presence of CO₂ will reduce the calorific value of natural gas.³ The currently available carbon capture materials lack its recyclability and cost-effectiveness also have large energy demand.⁴ Thus, the design and development of new carbon capture materials are important in the socio-economic point of view.

Metal-organic frameworks (MOFs) constitute a major class in the micro-mesoporous materials, with exceptional gas storage capacity.⁵ MOFs, due to its porous nature and tunability, can store a large amount of gas compared to the available materials.^{6,7} Also MOFs exhibit high chemical and thermal stability, with a potential application in CO₂ conversion. The chemical tunability of MOF-based materials make them competitive in the field of gas handling.⁸⁻¹⁰ But the selective adsorption is really needed for the separation of definite gases from the flue gas, which remains an unresolved problem for MOFs based separation process. Functionalization and mixed

Department of Chemistry, Faculty of Engineering and Technology, SRM Institute of Science and Technology, SRM Nagar, Kattankulathur, 603203, Chennai, TN, India. E-mail: prakashpm@gmail.com; prakashm4@srmist.edu.in

† Electronic supplementary information (ESI) available: Structure of ILs, ZIF-8 and ILs@ZIF-8, force field parameters for all the framework atoms and gas molecules. Computed He-void and PSD analysis of the composites. The adsorption isotherms of gases in ZIF-8 and composite materials. Selective gas adsorption in N-based anionic composites. Snapshots from various GCMC simulations. See DOI: 10.1039/d0ra07927h



matrix membranes (MMMs) helps to overcome this limitation of MOFs by enhancing the selective adsorption.^{11–13}

Various reports are available on MOF based materials for efficient and selective CO₂ capture.^{14–16} Here, we analyzed the effect of encapsulated ILs and role of their interaction with MOF in selective CO₂ adsorption from flue gas mixtures. It is well known that imidazolium-based ILs have widespread applications in different fields such as gas sensors, separation, energy storage and catalysis.^{17,18} ILs can also be incorporated in metal surfaces for electrochemical and various other applications.^{19,20} It has a high CO₂ solubility character which results in potential separation techniques.²¹ Also the recyclability of ILs helps in making them a better candidate for gas handling applications.²² Sezginel *et al.* studied CuBTC MOF with the incorporation of ILs for gas separation applications. But the gas separation was inversely affected, which is arisen from the interaction between ILs and open metal sites of MOF.²³ IL encapsulation in MOFs with saturated metal sites can significantly enhance the gas separation performance.^{24,25} Recently, Polat and co-workers, analyzed IL/CuBTC composite for the selective CO₂ separation. They found that IL incorporation can enhance the CO₂ selectivity of the material, with the help of experiments and simulations.²⁶ The high CO₂ selectivity of IL@IRMOF was reported by Gupta *et al.* using atomistic simulations.²⁷

Among the MOFs, zeolitic imidazolate framework is a subclass that has a sodalite (SOD) topology with flexible linker and tunable pore size.²⁸ ZIFs can be used in various applications such as chemical sensors, optical switch, biomedical applications, catalysis *etc.*^{29–31} Due to the wide variety of ZIFs and the superior CO₂ solubility of ILs, they can lead to the generation of an energy-efficient carbon capture material as well as these can be used for the membrane-based separation process.^{32,33} The modified linkers in these frameworks can also lead to efficient gas mixture separation.³⁴ Recent experimental and computational approaches show that the hydrophobic/hydrophilic character of ZIFs play a vital role in the efficient binding of guest molecules as well as possible gas storage and separation techniques.^{35–37} These studies reveal that the interactions at the interface are playing significant role in the composite stability as well as selective storage of gas molecules at nanopores.

ILs are proven to be efficient CO₂ soluble material, whereas ZIFs are emerged as good storage and separation material. Combining these two novel materials will help us to utilize the unique properties of these materials in one platform. Also, the IL@MOF can provide a good interfacial material for gas separation by combining the advantages of solid adsorption as well as liquid absorption.³⁸ These IL/MOF composites show better performance in many fields such as ionic conductivity, catalysis, membrane based separation *etc.*³⁹ Many studies have reported successful encapsulation of ILs into the confinement of porous materials and thus enhancing its CO₂ separation ability. The incorporated IL in ZIFs can avoid freezing up to a much lower temperature and thus can be used as low temperature ionic conductors.⁴⁰ Ban *et al.* incorporated IL into ZIF-8 confinement and observed an increasing permeability for CO₂ molecule, compared to CH₄ and N₂.³² Keskin and co-workers observed high CO₂/CH₄ selectivity for core-shell type IL@ZIF-

8 composite.³⁵ From these studies, it is clear that the modification of ZIFs with specific ILs can enhance the permeability and selectivity of desired gas molecules. Through the combination of ILs and ZIFs, we can design a stable and compatible material for selective gas adsorption from industrial flue gas. There are many experimental and theoretical reports available, which shows the effectiveness of ILs, confined in MOFs, for selective CO₂ adsorption.^{41–43} Recent trends show that porous ILs and IL-based composite materials are receiving widespread attention in the fields of gas storage, separation and catalysis.^{44–46}

Computational exploration of materials is always valuable because it can give a clear picture of microscopic interfacial interactions in newly designed materials. Thus, in the present study, we have employed computational approaches to screen various ILs at the ZIF-8 nanopores using DFT and GCMC simulations. Also the interfacial interactions between ZIF and ILs and their role in the effective gas separation are analyzed. Cadena *et al.* reported that the anion in the imidazolium ILs has a major part to play in the solubility of CO₂ in the same.²¹ So we have selected common 1-butyl-3-methylimidazolium ([BMIM]⁺) cation with various anions for ILs, to explore its effects in the stability as well as CO₂ separation. Insights into the microscopic interfacial interaction along with macroscopic characteristic features of the composite materials are very important to identify the selective gas adsorption and separation. The structure and stability of the composite materials have been characterized by the DFT with the Grimme's dispersion correction (DFT-D3).⁴⁷ Using the results from atomistic simulations, the stable composite materials were analyzed for its selective gas adsorption and storage applications. These computations were done by the force field based GCMC approach. Different force fields were used to compare our results with the available experimental results.^{24,25} Based on the observations, new composite materials were reported for the potential CO₂ storage and separation applications. Furthermore, our computational methodology can provide an atomic-scale perception of the interfacial interaction between ILs and ZIFs as well as selective CO₂ adsorption. Even though there are some previous reports on IL@ZIF-8, ours is the first one to analyze the role of anion and influence of interfacial interactions on the selective CO₂ capture. This study provides a systematic computational approach to identify the role of interfacial interactions in the selective CO₂ capture at IL based composites and this can be helpful in experimental/industrial design of such materials.

2. Computational methodology

2.1. DFT calculations

The geometries of all the ILs were optimized using Becke's three-parameter hybrid exchange functional and the Lee–Yang–Parr correlation functional (B3LYP)^{48,49} with 6-311++G** basis set in Gaussian16 package.⁵⁰ One IL ion-pair is incorporated into the pore of ZIF-8 and optimized using CELLOPT protocol to relax the composite structures. All the DFT periodic calculations are done using Quickstep package in CP2K⁵¹ version 5.1.



CELLOPT method helps in relaxing the structure by adjusting the original lattice parameters.³⁶ It helps to find the change in the cell volume with the incorporation of ILs in ZIF-8. For this optimization, PBE (Perdew–Burke–Ernzerhof)⁵² exchange correlation method is used with Grimme's D3⁴⁷ semi-empirical dispersion correction. Inclusion of dispersion correction has great influence on the prediction of properties of composite materials.³⁶ Also they are found to be effective in predicting the structure of various ZIFs.⁵³ So we have included D3 dispersion in order to describe the properties of ILs based membranes. A mixed Gaussian plane wave (GPW) basis set scheme was used to represent the pseudo potentials and valence electron density of the elements. All atoms, except B and Zn, were described by the MOLOPT-TZVP (triple-zeta valence polarized) basis set, whereas for zinc and boron atoms, MOLOPT-DZVP (double-zeta valence polarized) was used.⁵⁴ GTH (Goedecker–Teter–Hutter)⁵⁵ pseudo potentials were used for all atoms. The orbital transformation (OT) was used for the electronic energy minimization and plane wave cut off (450 Ry) was included. The adsorption energies (E_{ads}) for all the complexes are calculated from the optimized geometries using the following equation:

$$E_{\text{ads}} = E_{\text{total}} - (E_{\text{ZIF-8}} + E_{\text{IL}}) \quad (1)$$

where E_{total} , $E_{\text{ZIF-8}}$ and E_{IL} are the total energies of the composite, ZIF-8 and IL, respectively.

2.2. GCMC simulations

GCMC simulations are carried out at temperature 298 K to study single component adsorption isotherm of CO₂, N₂ and CH₄ as well as binary mixture (CO₂/N₂ and CO₂/CH₄ mixtures) selectivity of these gases in the pure ZIF-8 and composite materials. All calculations were done using RASPA⁵⁶ simulation package. Here, the interaction between composite and gas molecules (CO₂, N₂ and CH₄) were modeled using 12-6 Lennard-Jones (LJ) potential. Cross-atomic force field parameters were defined using Lorentz–Berthelot mixing rule given by, $\epsilon_{ij} = \sqrt{\epsilon_i \epsilon_j}$ and $\sigma_{ij} = (\sigma_i + \sigma_j)/2$ where ϵ_i and σ_i are the LJ parameters for the species *i*. Validation of different force field was done by comparing the results with the reported experimental isotherm.²⁴ Universal force field (UFF),⁵⁷ Dreiding force field⁵⁸ and GenericMOFs force fields⁵⁶ (as implemented in RASPA) were compared with the available experimental data. GenericMOFs is a mixed force field where the metal center (Zn) is treated by UFF and other atoms by Dreiding force field. The CO₂ and N₂ gas molecules were modeled as three site rigid model and CH₄ as single site model using TraPPE force field.⁵⁹ The force field parameters used for different framework atoms and gas molecules are given in Tables S1 and S2 (in ESI†). Pressure ranges from 0.01 to 10 bar were investigated at 298 K for each isotherm. Each simulation had 1×10^7 steps for initialization and 1×10^6 steps for equilibration. In single component simulations, four different moves were used, which are translation, rotation, reinsertion and swap. In binary mixture calculations, identity exchange was also considered along with these four moves. Equimolar binary mixtures (50/50) of CO₂/N₂ and CO₂/CH₄ were considered for

selective CO₂ adsorption. The selectivity (*S*) of these mixtures are calculated using the following equation:

$$S_{a/b} = \left(\frac{N_a}{N_b} \right) / \left(\frac{Y_a}{Y_b} \right) \quad (2)$$

where, *N* and *Y* are the amount adsorbed in bulk phase and mole fraction of the gas in the mixture respectively, for the gases *a* and *b*. To know the occupancy of ILs in ZIF-8 pores, we computed helium void fraction and pore-size distribution (PSD) of ILs@ZIF-8, and the same were compared with that of ZIF-8. Also, the heat of adsorption (ΔH_{ads}) is calculated for CO₂, N₂ and CH₄ at different composites and ZIF-8, at infinite dilution condition.

3. Results and discussion

3.1. Geometry and energetic of ILs@ZIF-8

A total of eleven ILs, both hydrophilic and hydrophobic, were incorporated to study the effect of anion in the nanopores for the selective CO₂ capture and separation application. For this, we have chosen [BMIM]⁺ cation with various hydrophilic/hydrophobic anions [X][−], where X = trifluoroacetate [CF₃CO₂][−], tetrafluoroborate [BF₄][−], hexafluorophosphate [PF₆][−], chloride [Cl][−], trifluoromethanesulfonate [OTF][−], dicyanamide [DCA][−], nitrite [NO₂][−], nitrate [NO₃][−], azide [N₃][−], thiocyanate [SCN][−] and bis(trifluoromethylsulfonyl)imide [Tf₂N][−]. These anions are experimentally known and can be easily incorporated into ZIF-8 pore. Few of these anions are already reported at the ZIF-8 nanopores to enhance the CO₂ adsorption.^{24,25,32,60} The optimized geometries of various ILs along with the important distance between ion-pairs (in Å) are given in Fig. 1. It is found that all the anions are directly hydrogen bonded (H-bonded) with C₂H group of [BMIM]⁺ cation. The calculated H-bonding distance between IL ion-pair varies from 1.75 to 2.33 Å, irrespective of nature of anions (*i.e.* hydrophobic/hydrophilic). In addition to this some of the anions were weakly H-bonded with alkyl group in [BMIM]⁺. The optimized geometry of ZIF-8 structure is shown in Fig. 2 along with the pore size (~11.95 Å). ILs are incorporated into this optimized ZIF-8. The geometry of selected IL ion-pairs, ZIF-8 structure, various ILs incorporated ZIF-8 complexes and PSD plots are provided in Fig. S1–S5 (in ESI†).

ILs are impregnated into the nanopores of ZIF-8 and optimized using PBE method with D3 dispersion correction. To find the stability and structural properties of ILs@ZIF-8 composite, we optimized all the complexes using DFT based periodic calculations. This approach can provide a clear picture of microscopic interfacial interaction between ILs and ZIF-8. Also the magnitude of the stability depends on the nature of interfacial charge transfer in the complex.³⁶ The shortest interacting distances between anion–cation and the framework, observed from the optimized geometries, are given in Table 1. In addition, the optimized geometries along with shortest interaction distances are provided in Fig. S3 (in ESI†). Even at the confined environment, the geometries of ILs are not disturbed and these ion-pairs are stabilized by the electrostatic interactions and H-bond(s). In addition, some of the IL ion-pairs have strongly



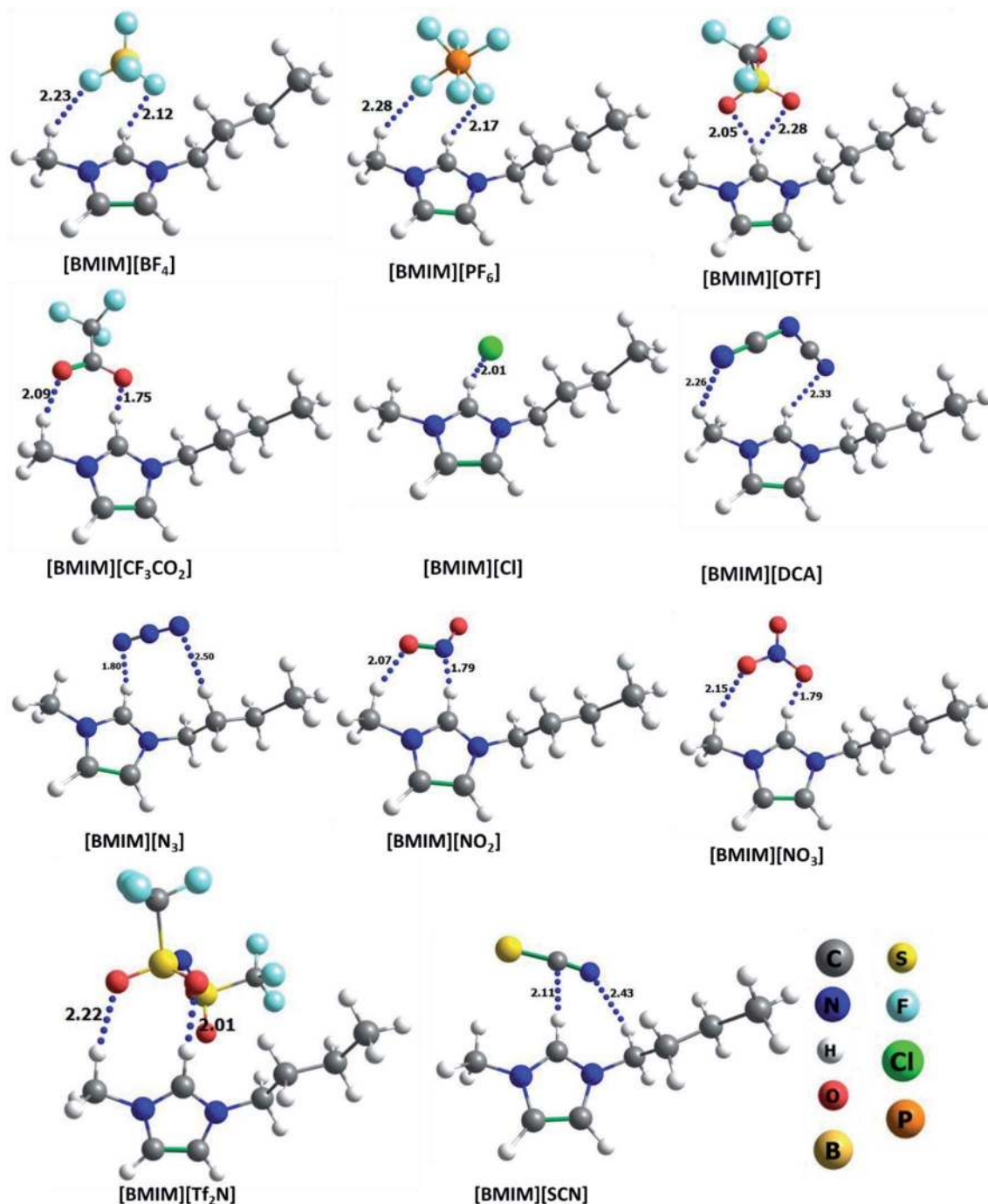


Fig. 1 Optimized geometries of monomers of all the ILs used in this study, along with shortest interaction distances between anion and cation (in Å).

interacted with ZIF-8 surface. The calculated interacting distance of cation-surface and anion-surface are varied from 2.32–2.70 Å and 2.37–4.04 Å, respectively. It is to be noted from the Fig. S3† that both anion and cation of fluorinated ILs are strongly interacting with the surface which significantly influences the calculated adsorption energies.

Also, the change in volume (in percentage) is calculated in comparison with the experimental crystal structure. The changes in unit cell parameters were closely analyzed after the

incorporation of ILs at the ZIF-8 nanopores. These parameters suggest that there are no significant structural changes in the ZIF-8 framework after encapsulation ILs. It can be noted that the average expansion of unit cell is ~1.8% with respect to the experimental crystal structure of ZIF-8. Furthermore, the volume expansion depends on the size of the anion. After optimization of composites, [BMIM]⁺ with [PF₆]⁻, [CF₃CO₂]⁻ and [OTF]⁻ anion containing structures are slightly expanded than the average cell volume (*i.e.* >2%). The significant



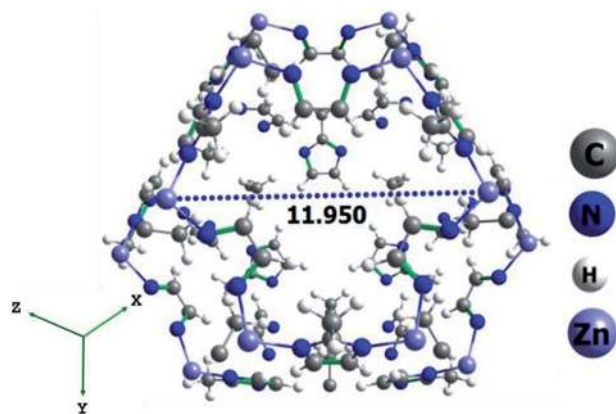


Fig. 2 The optimized geometry of ZIF-8 structure using CELLOPT method. The dotted line shows the pore cavity (in Å).

enhancement in the cell volume may arise from the influence of anions at the confined state. This is also reflected in the calculated adsorption energies of fluorinated anions. Higher adsorption energies of IL leads to more expansion in volume of ZIF-8 crystal structure, which is due to the existence of strong interfacial interaction between ILs and ZIF-8.

The interaction energies of the complexes can be quantified from the calculated E_{ads} between ILs and ZIF-8 structure. The dominant interfacial interactions can stabilize the ion-pair at the ZIF-8 nanopore. These interactions can predict the order of stability and the calculated magnitude of strength is provided in Table 1. The obtained results reveal that some of the ILs are not adsorbed on the surface of the ZIF-8. These ILs have a repulsive kind of interaction with the surface, *i.e.*, the ILs are showing positive E_{ads} . It is also interesting to note that all the ion pairs with a positive E_{ads} contain at least one nitrogen atom in the anion of IL (N-based ILs). The repulsive nature of these ILs may arise from the interaction of non-localized nitrogen lone-pair and the ZIF-8 imidazolate surface. The non-N based anion complexes are well adsorbed on the ZIF-8 surface (shown in ESI Fig. S4†). This is due to the attractive interfacial interaction

between ion-pair and surface (negative value for E_{ads}). Some recent studies investigated the IL@ZIF-8 complexes, but the structure, stability and interfacial interactions of series ILs based composite materials were not reported.^{26,60,61} Some of the N-based anions have shown high CO_2 solubility,⁶² but here we observed that they are incompatible and less stable at the ZIF-8 confinement. So in order to find the significance of these interfacial interactions in the gas adsorption/selectivity, we studied these composites using GCMC simulations and discussed in the following sections.

In the present study, we found the anion based selective adsorption of IL@ZIF-8, which is more dominant for gas sensing and separation applications. The stability of complex originates from the well-matched interfacial interaction between IL and ZIF-8. Our previous study showed that hydrophobic ZIFs prefer to stabilize the hydrophobic IL (*i.e.*, like-like pair).³⁶ Present work shows that not only like-like pair effect but also anionic part of the ILs plays a major role in the composite stability. This infers that anion in the selected ILs play a vital role in identifying the potential composite materials. It is interesting to note that, the fluorine atom(s) in the anion play a significant role in the capture of CO_2 molecules.³³ All the composites which were screened through DFT method were imposed for the adsorption and selective separation of CO_2 from CO_2/N_2 and CO_2/CH_4 binary mixtures using GCMC simulations.

3.2. GCMC simulations

3.2.1 Single component adsorption isotherms. CO_2 , N_2 and CH_4 gases were selected to analyze the adsorption capacity of the designed composite materials. The charges for framework atoms and ILs were calculated using charge equilibration method as implemented in RASPA and these charges are used in the adsorption studies. The helium void of all the composites are given in Table S3† and PSD of stable ILs@ZIF-8 complexes are provided in Fig. S5 (ESI†). The calculated charges for framework atoms as well as all the ILs considered in this study are given in Tables S4–S6 (in ESI†). PSD and He-void

Table 1 The calculated distances between anion and cation in ILs with the framework (in Å) along with the calculated adsorption energies of IL@ZIF-8 and the respective pore volume changes (in %)

[BMIM][X]@ZIF-8 composites	Shortest interacting distances (Å)			Change in cell volume (%)	E_{ads} (kcal mol ⁻¹)
	[BMIM] ⁺ –[X] [–]	ZIF-8 and [BMIM] ⁺	ZIF-8 and [X] [–]		
[BMIM][NO ₃]	1.78	2.53	2.61	1.49	32.91
[BMIM][TF ₂ N]	2.10	2.70	2.53	1.52	27.56
[BMIM][DCA]	2.25	2.44	4.04	1.61	26.94
[BMIM][N ₃]	1.67	2.36	2.96	1.68	16.79
[BMIM][SCN]	2.13	2.44	3.13	1.81	9.10
[BMIM][NO ₂]	1.81	2.43	2.70	1.79	4.37
[BMIM][Cl] ³⁶	2.11	2.34	2.87	1.93	–6.56
[BMIM][BF ₄] ³⁶	2.10	2.41	2.68	1.96	–9.90
[BMIM][CF ₃ CO ₂] ³⁶	1.77	2.49	2.43	2.05	–15.67
[BMIM][PF ₆] ³⁶	1.99	2.54	2.37	2.18	–31.72
[BMIM][OTf]	2.02	2.32	2.45	2.31	–43.52



calculations help to analyze the available free space in ZIF-8 with and without encapsulated ILs. They were reduced after IL incorporation in the ZIF-8, which clearly shows that the void space is partially occupied by IL and thus may reduce the uptake of gas molecules. But IL incorporation can enhance the selectivity of particular gas molecules at composites. After these calculations, the loading of CO₂, N₂ and CH₄ were calculated at constant temperature (*i.e.* 298 K) with varying pressure conditions.

The selection of suitable force field is important to predict the gas capture ability of the ZIFs.⁶³ To select suitable force field for molecular simulations and to confirm our results with experimental adsorption isotherm, we studied three different force fields such as UFF, Dreiding force field and GenericMOFs force field for CO₂ and N₂ gas molecules. For these gas molecules, three site rigid TraPPE model was used. The adsorption isotherms for empty ZIF-8 and IL loaded ZIF-8 (*i.e.*, 3[BMIM][PF₆]) in comparison with available experimental isotherms are shown in Fig. 3a and b, respectively. The previously reported experimental data correspond to 24 wt% of IL in ZIF-8 unit cell.²⁴ So, here we compared our results with the same wt%, which is equivalent to 3 ion-pairs of ILs per unit cell. It is interesting that among the three different force fields, the Dreiding force field is in very good agreement with the available experimental isotherm for the CO₂ and N₂@composite. Whereas in the case of pristine ZIF-8, GenericMOFs force field is more closely predicting the experimental results. Even though the GenericMOFs force field shows better agreement with the experiments for empty ZIF-8 crystal, Dreiding force field shows better results for both ZIF-8 and IL based composite materials. The results obtained from UFF were not so promising as compared to other two force fields. Thus, we focused on Dreiding force field to study the adsorption isotherm as well as co-adsorption selectivity of CO₂, N₂ and CH₄ in the composite materials. A similar result was observed by Polat *et al.* in their recent work on open metal site MOF (CuBTC)/IL composite.²⁶ Here, we observed analogous results for saturated MOF/IL composite. Using the predicted force field, new stable

composite materials were explored for its gas storage capacity and selectivity.

The comparison of adsorption isotherms of different non-N based stable composite materials is depicted in Fig. 4 for CO₂, N₂ and CH₄. The designed composite materials show higher gas uptake when compared to ZIF-8 at low pressure (≤ 3 bar) and 298 K. These conditions follow the optimum environment for the flue gas mixture separation.⁶⁴ In the plots presented in Fig. 4a, with an increase in the pressure, the isotherm of ZIF-8 are crossing over the isotherms of all composites. This is because of the accommodation of more number of gas molecules in the available ZIF-8 pore at higher pressure (≥ 5 bar). This is absent in ILs@ZIF-8 composite, because of the accumulation of ILs at the pores. In the isotherm plots of N₂ and CH₄ (Fig. 4b and c), there are no intense changes in the adsorption. The individual adsorption isotherms of CO₂, N₂ and CH₄ at stable composites are given in Fig. S6 (ESI†).

In order to analyze the effect of interaction energy in the gas storage of the complexes, we also analyzed the CO₂, N₂ and CH₄ gas adsorption isotherms of all N-based composites (Fig. S7 in ESI†). The comparison of isotherms for these composites is given in Fig. S8 in the ESI.† From the figure, it is clear that even though the ILs are not stable inside the ZIF-8 confinement, they still can accommodate large amount of gases, which is no less than the stable composites. The anions in the selected ILs have similar size and they have uniformly occupied the ZIF-8 pore. This is evident from He-void and PSD data. Due to the availability of pores, a large amount of gas (CO₂, N₂ and CH₄) can be adsorbed on the composites, irrespective of its interaction with ZIF-8. Also, we have added only one IL ion pair/ZIF-8 pore. So this can further enhance the gas adsorption by providing more vacant sites. The amount of gas adsorbed can be slightly varied according to the size of the anion. [BMIM][Tf₂N]@ZIF-8 has slightly lesser gas storage due to the larger anion size. From this it is clear that the interfacial interaction energies between different ILs and ZIF-8 do not affect the gas adsorption in these composites.

3.2.2 Separation of binary gas mixture at the composites.

To understand the CO₂ separation capability of the materials in

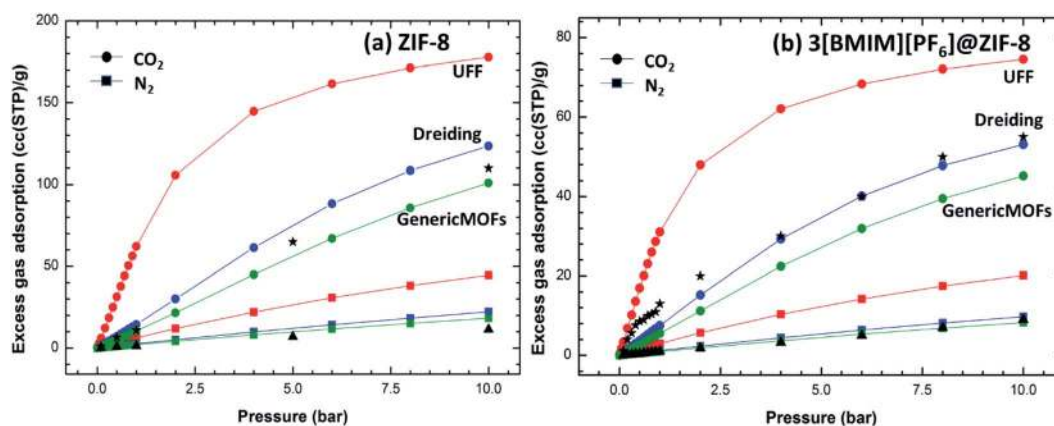


Fig. 3 Adsorption isotherm of (a) ZIF-8 and (b) 3[BMIM][PF₆]@ZIF-8 computed using different force fields in comparison with available experimental results (▲ and ★ represents experimental N₂ and CO₂ uptakes, respectively).



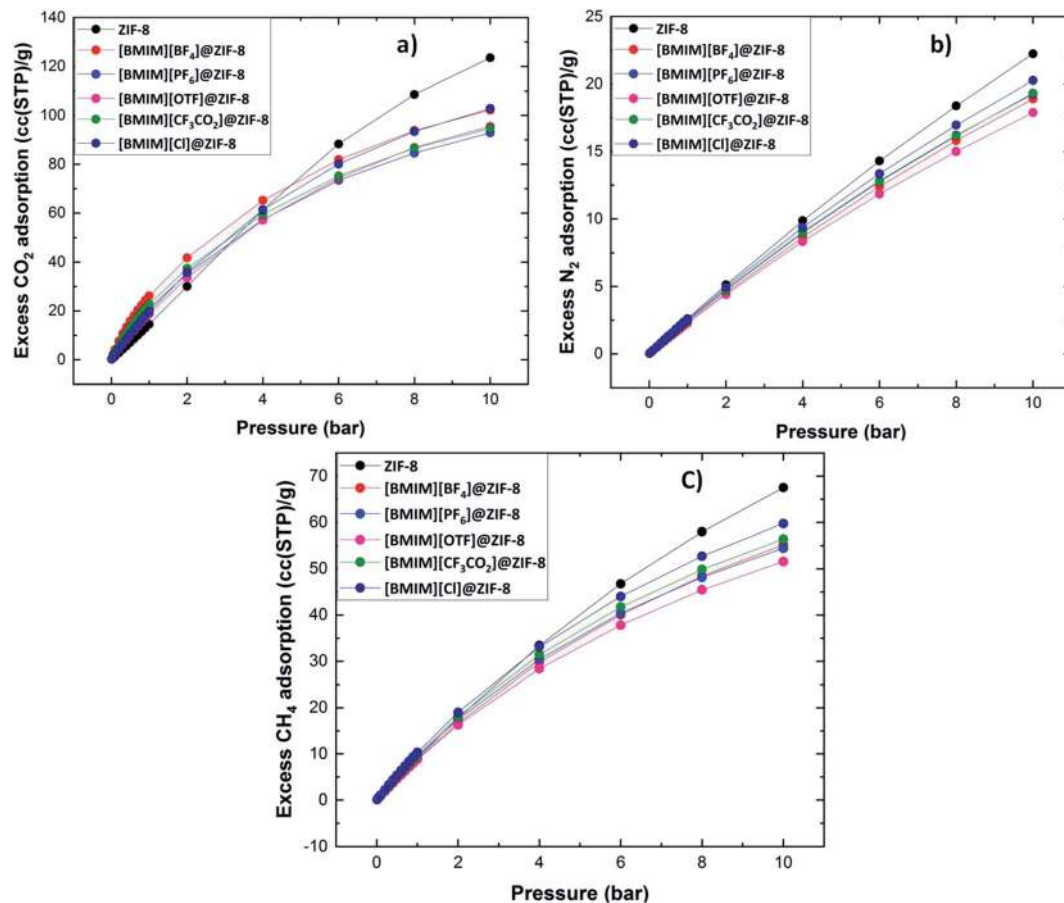


Fig. 4 Comparison of gas adsorption isotherm of ZIF-8 and non-N based anionic ILs@ZIF-8 composites were calculated using Dreiding force field for (a) CO_2 , (b) N_2 and (c) CH_4 .

real-time applications, the CO_2 selectivity was calculated from the binary mixture adsorption of CO_2/N_2 and CO_2/CH_4 at equimolar concentrations. The selective separation of CO_2 was identified from GCMC simulations. Fig. 5 gives a comparison of CO_2 selectivity from two different gas mixtures, for stable composites. Fig. 5a shows the CO_2/N_2 selectivity for different

composites. From the figure, it is clear that the designed composite material has better CO_2 selectivity compared to pristine ZIF-8. It is found that $[\text{BMIM}][\text{BF}_4]@ZIF-8$ complex has high CO_2 selectivity when compared to others. So our predicted materials show better selective adsorption towards CO_2 at the optimum experimental condition. The non-fluorinated $[\text{BMIM}]$

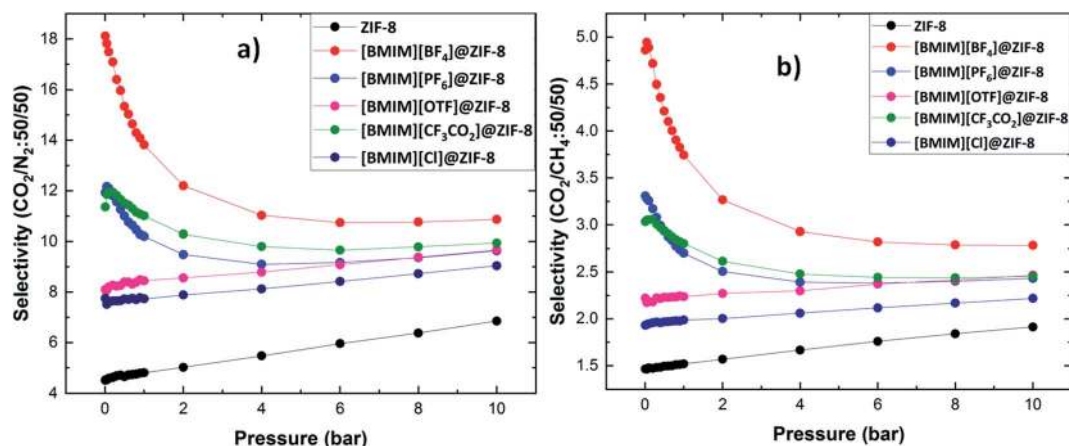


Fig. 5 The binary gas mixture selectivities of ZIF-8 and stable non-N based composite materials (a) CO_2/N_2 and (b) CO_2/CH_4 .



[Cl]@ZIF-8 has lower selectivity when compared to other materials. Even though $[Cl]^-$ anion is polar and has hydrophilic nature, fluorinated anions in IL-based composite shows the better selective adsorption of CO_2 . This is in well agreement with the calculated E_{ads} . These composites show higher selectivity at a lower pressure than higher pressure regions. This can be helpful in industrial flue gas separation. Fig. 5b shows the CO_2/CH_4 selectivity of the composites. The selective CO_2 adsorption is less from this gaseous mixture compared to CO_2/N_2 mixture. This mixture follows the similar trend as CO_2/N_2 mixture. $[BMIM][BF_4]$ @ZIF-8 shows highest selectivity for CO_2 among the composites. The IL incorporation has enhanced the CO_2 selectivity of ZIF-8. The fluorinated ILs show better selectivity compared to non-fluorinated $[Cl]^-$. From the interaction strength of ILs@ZIF-8 and selective CO_2 adsorption, it is clear that fluorinated anions in the IL can efficiently bind to the ZIF-8 surface and they also influence the CO_2 selective adsorption. It is also interesting that the selectivity of some ILs@ZIF-8 (*i.e.* $[BF_4]^-$, $[PF_6]^-$ and $[CF_3CO_2]^-$) reduces with increasing pressure, whereas for other ILs, the selectivity increases with increasing pressure. In these complexes, the selectivity is much higher at lower pressure, *i.e.* the amount of CO_2 adsorbed compared to other gases is higher at low pressure. But as the pressure increases, the CO_2 molecules occupy the pores and hence reduces the intake of incoming gas molecules. So the selectivity decreases as the pressure increases. But for the other composites, (*i.e.* pristine ZIF-8, $[OTf]^-$ and $[Cl]^-$ based complexes) the selectivity is less at low pressure. So the gas molecules adsorbed on the pores are also less. As the pressure increases, the more gas molecules will be accommodated into the pores. Especially CO_2 molecules, because our interface material has high affinity for CO_2 molecules. So as the pressure increases, there is a gradual increase in the selectivity for these anions.

In addition, the CO_2 selectivity for all the N-based ILs@ZIF-8 were analyzed. Fig. S9 in ESI† represents the binary mixture selectivities of different N-based ILs@ZIF-8 for CO_2/N_2 and CO_2/CH_4 mixtures. All the composites show better selective adsorption than pristine ZIF-8. From Fig. S9,† it is clear that $[BMIM][Tf_2N]$ @ZIF-8 shows comparatively higher selectivity despite of having a repulsive interaction with the surface. Even though they have repulsive interactions, all the N-based complexes show selectivity better than pristine ZIF-8. Compared to $[BMIM][Tf_2N]$ @ZIF-8 complex, other N-based IL complexes show lower selectivity. Recent reports on $[BMIM][Tf_2N]$ @ZIF-8 suggest that IL act as good cavity occupants in ZIF-8 and enhances the CO_2 selectivity.^{65,66}

Close analysis of both type of composites shows that the fluorine containing IL anions in the composites show better CO_2 adsorption and significant CO_2 selectivity than pristine ZIF-8, especially at low pressure. Irrespective of the nature of interaction between ILs and ZIF-8, the IL incorporation itself can enhance the CO_2 selectivity of ZIF-8. Particularly, the fluorine content with the combination of hydrophobic nature plays an important role in enhancing the CO_2 selectivity. Hydrophobic and fluorinated anions such as $[BF_4]^-$, $[Tf_2N]^-$ and $[PF_6]^-$ can enhance the selective separation of CO_2 compared to other anions used in this study. We previously reported that

there is an enhanced charge transfer between fluorinated ILs and ZIF-8.³⁶ This effective charge transfer can be helpful in strong interaction between CO_2 and ILs@ZIF-8. Even if the composites and pristine ZIF-8 show similar storage capacity, the selectivity is enhanced with the incorporation of ILs. This shows that the composite can store as much more gas molecules as the ZIF-8 with better CO_2 selectivity.

3.2.3 Heat of adsorption. The heat of adsorption indicates the strength of the interaction between adsorbate gas molecules and the adsorbent surface.⁶⁷ So quantifying the heat of adsorption can be helpful in the identification of role of IL (anion/cation) in the gas separation. So the heat of adsorption of ZIF-8 and non-N based composites at infinite dilution condition is calculated using the expression,⁵⁶

$$\Delta H_{ads} = \langle U_{gh} \rangle - \langle U_h \rangle - \langle U_g \rangle - RT \quad (3)$$

where, $\langle U_{gh} \rangle$, $\langle U_h \rangle$ and $\langle U_g \rangle$ are the average internal energies of the guest–host, host, and guest, respectively. R is the universal gas constant and T is the temperature (298 K). The comparison of $-\Delta H_{ads}$ for CO_2 , N_2 and CH_4 at different composites are given in Fig. 6. From the figure, it is clear that the heat of adsorption increases with IL incorporation. The pristine ZIF-8 has a ΔH_{ads} of -15.38 , -10.19 and -13.43 $kJ\ mol^{-1}$ for CO_2 , N_2 and CH_4 , respectively. But, the incorporation of IL into ZIF-8 enhances the ΔH_{ads} of the gas molecules at the composites. For CO_2 gas molecule, the heat of adsorption follows the order, $[BF_4]^- > [PF_6]^- \sim [CF_3CO_2]^- > [OTf]^- > [Cl]^- > ZIF-8$. After IL incorporation, there is a clear enhancement in the ΔH_{ads} of CO_2 than N_2 and CH_4 . There is only slight enhancement in the ΔH_{ads} of CH_4 and N_2 , after IL incorporation. This is due to the strong interaction of CO_2 with the framework compared to other two gases. This can be favorable in CO_2 adsorption from different gas mixtures. The non-fluorinated $[BMIM][Cl]$ @ZIF-8 has less heat of adsorption when compared to other fluorinated anions. From this, it is evident that fluorine content in the anion has a major role in the affinity of CO_2 molecules towards composites. The incoming CO_2 molecules form strong non-covalent interactions with the ion-pair and thus enhancing the heat of adsorption.

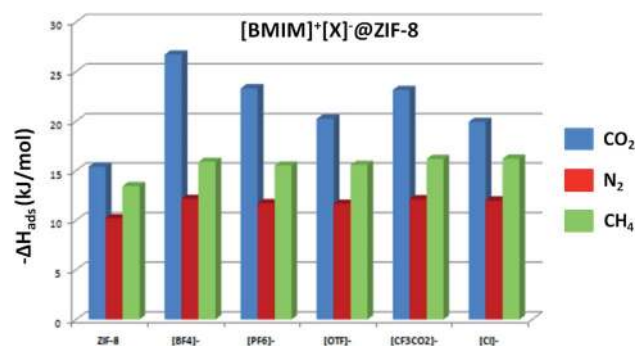


Fig. 6 The heat of adsorption calculated for CO_2 (blue), N_2 (red) and CH_4 (green) at ZIF-8 and different composites, at infinite dilution condition.



Fig. 7 shows the adsorption of CO₂ at ZIF-8 and the site-selective adsorption of CO₂ in the [BMIM][BF₄]@ZIF-8 complex. From the snapshots of GCMC simulations at different pressure, it is clear that the adsorbed CO₂ molecule is strongly interacting with the fluorine atom in the anion and alkyl chain of the cation. The oxygen in CO₂ interacts with hydrogen atom of alkyl chain in the cation through C–H···O H-bonds. This non-covalent interaction distance is ~3.0 Å. This is the reason for the enhancement in heat of adsorption after IL incorporation, which contributes to the better CO₂ selectivity of these materials. The shortest interaction distance between CO₂ and IL shows the site of adsorption and the role of fluorinated anion in the selective CO₂ capture at the ZIF-8 nanoconfinement. This attributes to the higher CO₂ selectivity of composites at low pressure and ambient temperatures. Also, from the binary mixture adsorption (Fig. S10†), it can be found that the incoming CO₂ forms a strong H-bond (~1.75 Å) with the BMIM⁺ cation of IL. This will lead to efficient storage and separation of CO₂ in the IL based composite than the bare ZIF-8. This proves that the designed material show high CO₂ selectivity due to the strong interfacial interactions between gas molecules and composites. Yang and co-workers reported that, at zero pressure, the selectivity depends on the difference in isosteric heats and independent of the material and gas mixtures.⁶⁸ By incorporation of ILs to the ZIF-8 nanopore, we can enhance the selective adsorption of CO₂. Since the heat of adsorption is more for the fluorinated ILs, we can infer that the anion in ILs play a major role in selective CO₂ capture. It is found from our calculations that, the nature of anion and also

the number fluorine atom(s) in the anion plays a vital role in the CO₂ selectivity of the composites, irrespective of their interaction with ZIF-8 framework. The selection of suitable ILs directly leads to the enhancement of CO₂ adsorption as well as selectivity. These findings are observed from the combined DFT based computational screening and GCMC simulations approaches.

4. Conclusions

In summary, atomistic simulations were used to identify the interfacial interaction between different ILs and ZIF-8 and also their effect on selective CO₂ capture. We combined both DFT and GCMC approaches to identify better composite material. Adsorption energies quantified from DFT calculations suggest that some of the anions are not well adsorbed on the ZIF-8 surface. These anions contain nitrogen in it and the repulsive nature of lone pair of nitrogen leads to less compatible structure. In order to find out the role of these interfacial interactions in gas adsorption and selective CO₂ separation in these complexes, they were studied using GCMC simulations. Different existing force fields were validated with experimental results and Dreiding force field was found to give a better description of the ILs@ZIF-8. Further analysis of adsorption isotherms proved that the interfacial interaction does not affect the gas storage capacity of the composites. The CO₂/N₂ and CO₂/CH₄ selectivity is enhanced in the IL incorporated ZIF-8. Irrespective of the nature of interaction between ILs and ZIF-8, the IL@ZIF-8 shows improved CO₂ separation. Especially the CO₂

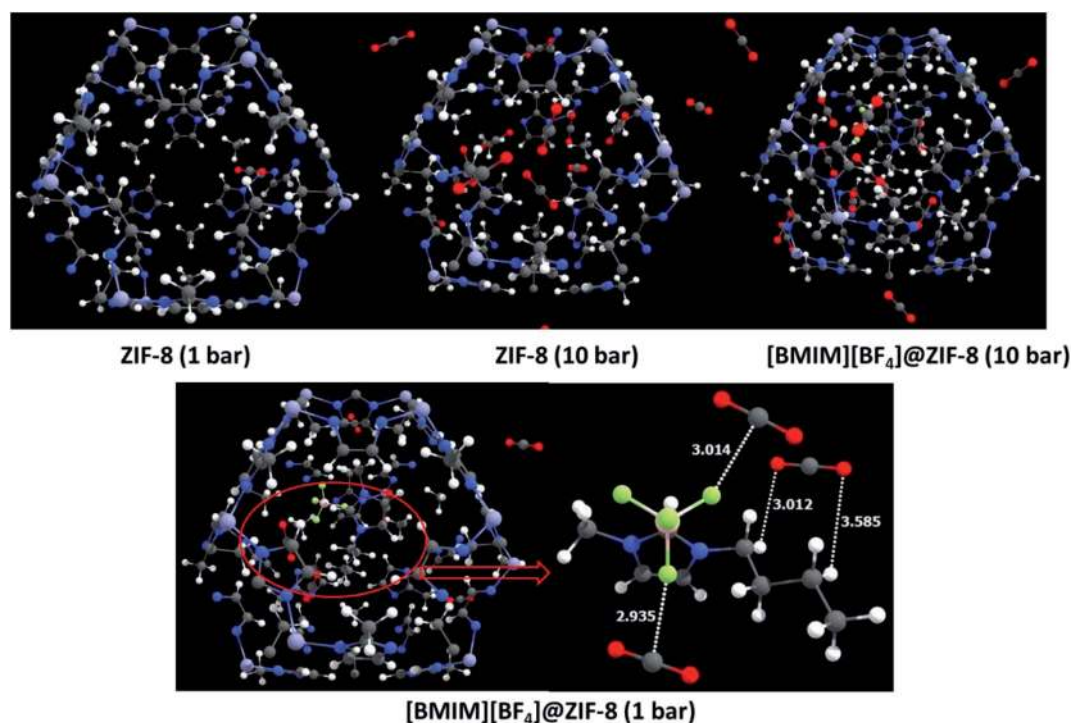


Fig. 7 Snapshots show the adsorption of CO₂ at bare ZIF-8 and [BMIM][BF₄]@ZIF-8 at different pressure (1 and 10 bar). The bottom figure shows the site selective adsorption of CO₂ at IL@ZIF-8 along with the shortest interacting distances (Å) of CO₂.



selectivity of hydrophobic fluorinated anions is much better compared to hydrophilic/non-fluorinated anions. Anions such as $[\text{BF}_4]^-$, $[\text{TF}_2\text{N}]^-$ and $[\text{PF}_6]^-$ improve the selective CO_2 separation, which is also confirmed from the enhanced heat of adsorption for CO_2 . Atomistic simulation based screening and identification of suitable composites for CO_2 capture can be a useful tool in real-time industrial flue gas separation.

Conflicts of interest

There are no conflicts of interest to declare.

Acknowledgements

M. P. thanks the Department of Science and Technology-Science and Engineering Research Board (DST-SERB) of India for the financial support (Grant number: ECR/2017/000891). A. T. thanks DST-SERB for the fellowship for her research work. The authors also thank SRM-IST for providing the super-computing facility and financial support.

References

- S. Solomon, G. K. Plattner, R. Knutti and P. Friedlingstein, *Proc. Natl. Acad. Sci. U. S. A.*, 2009, **106**, 1704–1709.
- Emissions gap report 2019*, United Nations Environment Programme (UNEP), Nairobi, 2019.
- M. Chawla, H. Saulat, M. Masood Khan, M. Mahmood Khan, S. Rafiq, L. Cheng, T. Iqbal, M. I. Rasheed, M. Z. Farooq, M. Saeed, N. M. Ahmad, M. B. Khan Niazi, S. Saqib, F. Jamil, A. Mukhtar and N. Muhammad, *Chem. Eng. Technol.*, 2020, **43**, 184–199.
- P. Markewitz, W. Kuckshinrichs, W. Leitner, J. Linsen, P. Zapp, R. Bongartz, A. Schreiber and T. E. Müller, *Energy Environ. Sci.*, 2012, **5**, 7281–7305.
- H.-C. Zhou, J. R. Long and O. M. Yaghi, *Chem. Rev.*, 2012, **112**, 673–674.
- R. E. Morris and P. S. Wheatley, *Angew. Chem., Int. Ed.*, 2008, **47**, 4966–4981.
- M. Prakash, H. Jobic, N. A. Ramsahye, F. Nouar, D. Damasceno Borges, C. Serre and G. Maurin, *J. Phys. Chem. C*, 2015, **119**, 23978–23989.
- M. Ding, R. W. Flaig, H. L. Jiang and O. M. Yaghi, *Chem. Soc. Rev.*, 2019, **48**, 2783–2828.
- F. Salles, H. Jobic, G. Maurin, M. M. Koza, P. L. Llewellyn, T. Devic, C. Serre and G. Férey, *Phys. Rev. Lett.*, 2008, **100**, 245901.
- D. Damasceno Borges, M. Prakash, N. A. Ramsahye, P. L. Llewellyn, S. Surblé, P. Horcajada, C. Serre and G. Maurin, *Mol. Simul.*, 2015, **41**, 1357–1370.
- B. Ghalei, K. Sakurai, Y. Kinoshita, K. Wakimoto, A. P. Isfahani, Q. Song, K. Doitomi, S. Furukawa, H. Hirao, H. Kusuda, S. Kitagawa and E. Sivaniah, *Nat. Energy*, 2017, **2**, 17086.
- M. Benzaqui, R. Semino, N. Menguy, F. Carn, T. Kundu, J. M. Guigner, N. B. McKeown, K. J. Msayib, M. Carta, R. Malpass-Evans, C. Le Guillouzer, G. Clet, N. A. Ramsahye, C. Serre, G. Maurin and N. Steunou, *ACS Appl. Mater. Interfaces*, 2016, **8**, 27311–27321.
- R. Semino, N. A. Ramsahye, A. Ghoufi and G. Maurin, *ACS Appl. Mater. Interfaces*, 2016, **8**, 809–819.
- B. Seoane, J. Coronas, I. Gascon, M. E. Benavides, O. Karvan, J. Caro, F. Kapteijn and J. Gascon, *Chem. Soc. Rev.*, 2015, **44**, 2421–2454.
- Y. Liu, J. Liu, M. Chang and C. Zheng, *J. Phys. Chem. C*, 2012, **116**, 16985–16991.
- N. A. Ramsahye, G. Maurin, S. Bourrelly, P. L. Llewellyn, T. Loiseau, C. Serre and G. Férey, *Chem. Commun.*, 2007, 3261–3263.
- C. P. Fredlake, J. M. Crosthwaite, D. G. Hert, S. N. V. K. Aki and J. F. Brennecke, *J. Chem. Eng. Data*, 2004, **49**, 954–964.
- J. E. Bara, T. K. Carlisle, C. J. Gabriel, D. Camper, A. Finotello, D. L. Gin and R. D. Noble, *Ind. Eng. Chem. Res.*, 2009, **48**, 2739–2751.
- S. Kamalakannan, M. Prakash, M. M. Al-Mogren, G. Chambaud and M. Hochlaf, *J. Phys. Chem. C*, 2019, **123**, 15087–15098.
- K. R. Maiyelvaganan, S. Kamalakannan and M. Prakash, *Appl. Surf. Sci.*, 2019, **495**, 143538.
- C. Cadena, J. L. Anthony, J. K. Shah, T. I. Morrow, J. F. Brennecke and E. J. Maginn, *J. Am. Chem. Soc.*, 2004, **126**, 5300–5308.
- B. Wu, W. W. Liu, Y. M. Zhang and H. P. Wang, *Chem. – Eur. J.*, 2009, **15**, 1804–1810.
- K. B. Sezginel, S. Keskin and A. Uzun, *Langmuir*, 2016, **32**, 1139–1147.
- F. P. Kinik, C. Altintas, V. Balci, B. Koyuturk, A. Uzun and S. Keskin, *ACS Appl. Mater. Interfaces*, 2016, **8**, 30992–31005.
- B. Koyuturk, C. Altintas, F. P. Kinik, S. Keskin and A. Uzun, *J. Phys. Chem. C*, 2017, **121**, 10370–10381.
- H. M. Polat, M. Zeeshan, A. Uzun and S. Keskin, *Chem. Eng. J.*, 2019, **373**, 1179–1189.
- K. M. Gupta, Y. Chen, Z. Hu and J. Jiang, *Phys. Chem. Chem. Phys.*, 2012, **14**, 5785–5794.
- K. S. Park, Z. Ni, A. P. Cote, J. Y. Choi, R. Huang, F. J. Uribe-Romo, H. K. Chae, M. O’Keeffe and O. M. Yaghi, *Proc. Natl. Acad. Sci. U. S. A.*, 2006, **103**, 10186–10191.
- A. Razmjou, M. Asadnia, O. Ghaebi, H. C. Yang, M. Ebrahimi Warkiani, J. Hou and V. Chen, *ACS Appl. Mater. Interfaces*, 2017, **9**, 38076–38080.
- L. Gao, Q. Chen, T. Gong, J. Liu and C. Li, *Nanoscale*, 2019, **11**, 21030–21045.
- A. Jamal Sisi, M. Fathinia, A. Khataee and Y. Orooji, *J. Mol. Liq.*, 2020, **308**, 113018.
- Y. Ban, Z. Li, Y. Li, Y. Peng, H. Jin, W. Jiao, A. Guo, P. Wang, Q. Yang, C. Zhong and W. Yang, *Angew. Chem., Int. Ed.*, 2015, **54**, 15483–15487.
- M. Mohamedali, H. Ibrahim and A. Henni, *Chem. Eng. J.*, 2018, **334**, 817–828.
- P. Krokidas, S. Moncho, E. N. Brothers, M. Castier, H. K. Jeong and I. G. Economou, *ACS Appl. Mater. Interfaces*, 2018, **10**, 39631–39644.



- 35 M. Zeeshan, V. Nozari, M. B. Yagci, T. Islk, U. Unal, V. Ortalan, S. Keskin and A. Uzun, *J. Am. Chem. Soc.*, 2018, **140**, 10113–10116.
- 36 A. Thomas, K. R. Maiyelvaganan, S. Kamalakannan and M. Prakash, *ACS Omega*, 2019, **4**, 22655–22666.
- 37 A. Thomas and M. Prakash, *Appl. Surf. Sci.*, 2019, **491**, 633–639.
- 38 X. Wang, D. Shang, S. Zeng, Y. Wang, X. Zhang, X. Zhang and J. Liu, *J. Chem. Thermodyn.*, 2019, **128**, 415–423.
- 39 F. P. Kinik, A. Uzun and S. Keskin, *ChemSusChem*, 2017, **10**, 2842–2863.
- 40 K. Fujie, K. Otsubo, R. Ikeda, T. Yamada and H. Kitagawa, *Chem. Sci.*, 2015, **6**, 4306–4310.
- 41 X. Xia, G. Hu, W. Li and S. Li, *ACS Appl. Nano Mater.*, 2019, **2**, 6022–6029.
- 42 L. G. Ding, B. J. Yao, W. L. Jiang, J. T. Li, Q. J. Fu, Y. A. Li, Z. H. Liu, J. P. Ma and Y. Bin Dong, *Inorg. Chem.*, 2017, **56**, 2337–2344.
- 43 Y. Chen, Z. Hu, K. M. Gupta and J. Jiang, *J. Phys. Chem. C*, 2011, **115**, 21736–21742.
- 44 S. Liu, J. Liu, X. Hou, T. Xu, J. Tong, J. Zhang, B. Ye and B. Liu, *Langmuir*, 2018, **34**, 3654–3660.
- 45 S. Zhang, J. Zhang, Y. Zhang and Y. Deng, *Chem. Rev.*, 2017, **117**, 6755–6833.
- 46 M. Costa Gomes, L. Pison, C. Červinka and A. Padua, *Angew. Chem., Int. Ed.*, 2018, **57**, 11909–11912.
- 47 S. Grimme, J. Antony, S. Ehrlich and H. Krieg, *J. Chem. Phys.*, 2010, **132**, 154104.
- 48 A. D. Becke, *Phys. Rev. A*, 1988, **38**, 3098–3100.
- 49 A. D. Becke, *J. Chem. Phys.*, 1993, **98**, 5648–5652.
- 50 M. J. Frisch, G. W. Trucks, H. B. Schlegel, G. E. Scuseria, M. A. Robb, J. R. Cheeseman, G. Scalmani, V. Barone, G. A. Petersson, H. Nakatsuji, X. Li, M. Caricato, A. V. Marenich, J. Bloino, B. G. Janesko, R. Gomperts, B. Mennucci, H. P. Hratchian, J. V. Ortiz, A. F. Izmaylov, J. L. Sonnenberg, D. Williams-Young, F. Ding, F. Lipparini, F. Egidi, J. Goings, B. Peng, A. Petrone, T. Henderson, D. Ranasinghe, V. G. Zakrzewski, J. Gao, N. Rega, G. Zheng, W. Liang, M. Hada, M. Ehara, K. Toyota, R. Fukuda, J. Hasegawa, M. Ishida, T. Nakajima, Y. Honda, O. Kitao, H. Nakai, T. Vreven, K. Throssell, J. A. Montgomery Jr, J. E. Peralta, F. Ogliaro, M. J. Bearpark, J. J. Heyd, E. N. Brothers, K. N. Kudin, V. N. Staroverov, T. A. Keith, R. Kobayashi, J. Normand, K. Raghavachari, A. P. Rendell, J. C. Burant, S. S. Iyengar, J. Tomasi, M. Cossi, J. M. Millam, M. Klene, C. Adamo, R. Cammi, J. W. Ochterski, R. L. Martin, K. Morokuma, O. Farkas, J. B. Foresman and D. J. Fox, *Gaussian 16, Revision A.03*, Wallingford, CT, 2016.
- 51 J. Vandevondele, M. Krack, F. Mohamed, M. Parrinello, T. Chassaing and J. Hutter, *Comput. Phys. Commun.*, 2005, **167**, 103–128.
- 52 J. P. Perdew, K. Burke and M. Ernzerhof, *Phys. Rev. Lett.*, 1996, **77**, 3865.
- 53 R. Galvelis, B. Slater, A. K. Cheetham and C. Mellot-Draznieks, Comparison of the relative stability of zinc and lithium-boron zeolitic imidazolate frameworks, *CrystEngComm*, 2012, **14**, 374–378.
- 54 J. VandeVondele and J. Hutter, *J. Chem. Phys.*, 2007, **127**, 114105.
- 55 S. Goedecker, M. Teter and J. Hutter, *Phys. Rev. B: Condens. Matter Mater. Phys.*, 1996, **54**, 1703.
- 56 D. Dubbeldam, S. Calero, D. E. Ellis and R. Q. Snurr, *Mol. Simul.*, 2016, **42**, 81–101.
- 57 A. K. Rappé, C. J. Casewit, K. S. Colwell, W. A. Goddard and W. M. Skiff, *J. Am. Chem. Soc.*, 1992, **114**, 10024–10035.
- 58 S. L. Mayo, B. D. Olafson and W. A. Goddard, *J. Phys. Chem.*, 1990, **94**, 8897–8909.
- 59 J. J. Potoff and J. I. Siepmann, *AIChE J.*, 2001, **47**, 1676–1682.
- 60 M. Zeeshan, S. Keskin and A. Uzun, *Polyhedron*, 2018, **155**, 485–492.
- 61 A. M. O. Mohamed, S. Moncho, P. Krokidas, K. Kakosimos, E. N. Brothers and I. G. Economou, *Mol. Phys.*, 2019, **117**, 3791–3805.
- 62 J. L. Anthony, J. L. Anderson, E. J. Maginn and J. F. Brennecke, *J. Phys. Chem. B*, 2005, **109**, 6366–6374.
- 63 M. Prakash, N. Sakhavand and R. Shahsavari, *J. Phys. Chem. C*, 2013, **117**, 24407–24416.
- 64 Z. Zhang, Y. Zhao, Q. Gong, Z. Li and J. Li, *Chem. Commun.*, 2013, **49**, 653–661.
- 65 A. Mohamed, P. Krokidas and I. G. Economou, *J. Comput. Sci.*, 2018, **27**, 183–191.
- 66 A. M. O. Mohamed, P. Krokidas and I. G. Economou, *Mol. Syst. Des. Eng.*, 2020, **5**, 1230–1238.
- 67 S. Builes, S. I. Sandler and R. Xiong, *Langmuir*, 2013, **29**, 10416–10422.
- 68 Z. Yang, X. Peng and D. Cao, *J. Phys. Chem. C*, 2013, **117**, 8353–8364.

